Noise Reduction Mechanisms in Supersonic Jets with Porous Centerbodies

V. Kibens* and R. W. Wlezien†
McDonnell Douglas Corporation, St. Louis, Missouri

An experimental investigation was performed to characterize changes in jet flowfield properties associated with noise reduction obtained using nozzles with porous centerbodies at supersonic pressure ratios. A series of constant-exit-area nozzles with various centerbody sizes was investigated over the Mach number range $0.8 \leq M \leq 1.4$. Periodic shock cells were observed in the flow for a nonporous centerbody. For a porous surface, the shock cells are replaced by a gradual compression composed of multiple weak shocks originating at the surface holes. Reduction of far-field jet noise correlates with a decrease of the pressure cell strength.

Introduction

THE concept of reducing supersonic jet noise by use of a nozzle with a porous centerbody was introduced by Maestrello.[1,2] The porous-centerbody nozzle is adaptable for use with turbofan engines by extending the rear bearing shields. In this application it must be redesigned in the form of a thrust-optimized "plug nozzle," which minimizes the nozzle length and weight while ensuring proper expansion of the flow along the plug surface. Optimized plug nozzles with and without porosity have been extensively studied by Dosanjh and his co-workers.[3]

Maestrello[2] showed that the noise from a porous-centerbody nozzle at supersonic pressure ratios is significantly lower than that from a comparable axisymmetric nozzle. He also observed noise reduction at subsonic pressure ratios. Maestrello concluded that the reduction in overall noise is primarily attributable to the elimination of shock-associated noise. His shadowgraph visualization data indicated that the core flow is essentially shock-free, and he suggested that shock intensity is reduced because 1) the surface porosity equalizes the static pressure across impinging shocks and expansion waves, thereby reducing the strength of their reflections, and 2) the flow geometry is modified from an axisymmetric circular jet to an annular wall jet along the centerbody. As the centerbody-to-nozzle diameter ratio is increased, the annular flow becomes more nearly two-dimensional, and the compression wave intensification or focusing that occurs at the center of a circular jet is suppressed.

Sound-generation mechanisms in supersonic axisymmetric jets have been studied extensively. Seiner and Norum[4] have shown that in an axisymmetric jet noise-generation intensity increases with streamwise distance and reaches a maximum between the third and sixth shock cells. Their results, as well as those of Pao and Seiner[5] and Seiner and Yu,[6] indicate that the predominant source of broadband noise is the interaction between the vortical structure in the thick shear layer and the intense pressure gradients associated with the shock cells. Lighthill[7] and Howe and Ffowcs Williams[8] have developed theoretical methods to address the shock/shear-layer interaction mechanism. Observations made by Tanna et al.[9] for coannular flows show that major reduction in noise is associated with the elimination of the highly organized shock structure present in the outer flow when the core flow is operated slightly above the critical pressure ratio.

The central intent of the present study was to identify mechanisms whereby a porous-centerbody surface causes noise attenuation and thus begin to characterize details of the processes involved. The study was performed as an adjunct to a parametric investigation of acoustic effects for a series of nozzle configurations performed by the Douglas Aircraft Company (DAC). Results of the acoustical surveys and direct thrust measurements for a series of porous-centerbody nozzles are described by Bauer,[10] and details of the entire program are presented in Ref. 11.

Experimental Apparatus and Approach

The porous-centerbody nozzles used for this study consisted of a subset of those tested by DAC, selected to investigate primarily the effects of porosity. The nozzles selected had been shown effective in suppressing noise. We chose three nozzles with the same centerbody diameter and a variation of porosity from 0 to 6%, a nozzle with a smaller centerbody to study the effect of annular height, and a reference nozzle without a centerbody. The nozzles described in detail below have equal exit areas and long, cylindrical centerbodies with nozzle exit walls parallel to the system axis. They generate strong initial shock systems that are needed to effectively study the noise attenuation mechanisms.

A 14% scale model of the General Electric CF6-50 engine primary exhaust system was common to all test configurations. It consists of a symmetrical centerbody held concentric with a constant-diameter duct by a set of eight radial struts. Figure 1 shows a schematic of a typical nozzle and centerbody arrangement. The nozzles and centerbodies downstream of the strut assembly were interchangeable. The nozzle test assembly was attached to a flow system consisting of a settling chamber and a conical contraction section with a downstream end faired into the test assembly. Dry, unheated air was supplied from large storage bottles, and the nozzles were exhausted into ambient air. The pumping capacity of the replenishment compressors was sufficient to permit steady-state operation. Constant mass flow rates were maintained through a digital valve system. Operational parameters and test data were recorded in an adjacent control room using an on-site digital data acquisition system.

Nozzle configurations are described in Table 1; for consistency, the configuration numbers used in the original nozzle designation scheme of Refs. 10 and 11 are retained. The two porosity values, $\sigma = 0.027$ and 0.056, are referred to as 3 and 6% porosity, respectively. Configuration 2 is a Mach 1.3 axi-

Presented as Paper 83-0774 at the AIAA Eighth Aeroacoustics Conference, Atlanta, Ga., April 11-13, 1983; received July 1, 1983; revision received Aug. 27, 1984.

*Senior Scientist, McDonnell Douglas Research Laboratories. Associate Fellow AIAA.

†Research Scientist, McDonnell Douglas Research Laboratories. Member AIAA.

symmetric reference nozzle, which produces a classic diamond-shaped shock system when operated at off-design conditions. Its well-defined shock structure was also used to evaluate the performance of the static-pressure probe. Configurations 6 and 10 were most efficient in suppressing the sound at the 0.53 and 0.80 centerbody-to-nozzle diameter ratios, respectively. Configuration 9T is geometrically identical to configuration 10 but has zero porosity. Configuration 8 has a surface porosity between those of configurations 9T and 10 and also offers a direct comparison with configuration 6 in measuring the effect of the centerbody-to-nozzle diameter ratio.

The experiments focused on the nominal variation of porosity, but the available set of nozzles did not permit the effects of extraneous parameters to be completely eliminated. For example, for nozzles 8 and 10 a porosity change of 3-6% is accompanied by a change in the centerbody length. Since our main object of study was the flowfield near the nozzle exit, we considered the effect of porosity to be dominant.

The flowfield experiments were conducted at five nozzle-pressure ratios (1.6, 2.2, 2.8, 3.4, and 4.0). Figure 2 shows the experimental apparatus with the LDV beam near the surface of a configuration 10 centerbody. Experimental data consisted of 1) streamwise and radial components of mean velocity, turbulence intensities, and turbulent Reynolds stress, obtained using a two-component laser-Doppler-velocimeter system (LDV); 2) instantaneous photographs and high-speed movies of shadowgraph images; 3) centerbody surface and flowfield static pressures, from static-pressure surface ports and a traversing static pressure probe, respectively; and 4) near-field sound pressure levels measured using condenser microphones.

Velocity Measurements

To perform LDV measurements, the jet and the entrained external air were seeded with atomized dioctyl phthalate, with a mean droplet diameter of 0.8 μm. The two-component LDV system used a 4-W argon-ion laser with maximum power at wavelengths of 514.5 nm (green) and 488.0 nm (blue) in a two-color, dual-beam, off-axis, forward-scatter mode. The fringe patterns were oriented 45 deg to the streamwise direction, allowing the system to detect the sum and the difference of the instantaneous streamwise and radial velocity components. The streamwise and radial velocity components were then recovered by adding and subtracting, respectively, the measured quantities. LDV measurements were limited to nozzle-pressure ratios less than 3.4 to avoid velocity biases caused by the condensation of water droplets from moisture in the entrained air.

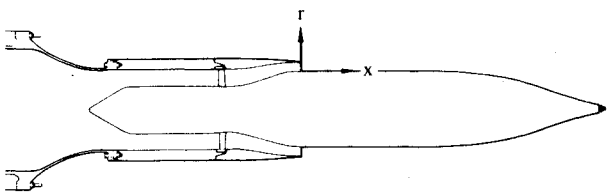

Fig. 1 Nozzle test assembly shown with configuration 10 porous-centerbody nozzle.

Table 1 Geometric parameters of test configurations

Configuration	d_1/d	d_0/d_1	ℓ_c/d	ℓ/d	σ	t/d
2	1.0	0	0	0	0	
6	1.18	0.53	2.0	3.45	0.027	0.0194
8	1.67	0.80	0.5	3.65	0.027	0.0065
9T	1.67	0.80	2.0	5.15	0	
10	1.67	0.80	2.0	5.15	0.056	0.0065

NB: d = diameter of equivalent circular nozzle, = 11.77 cm; d_1 = diameter of nozzle at exhaust plane; d_0 = diameter of plug at exhaust plane; ℓ = length of plug from exhaust plane; ℓ_c = length of constant diameter portion of plug from exhaust plane; σ = porosity (ratio of hole cross section to plug surface area; hole diameter = 0.168 cm); t = plug wall thickness.

Static-Pressure Measurements

Detailed static-pressure measurements were taken throughout the core flow using a static-pressure probe of the double conic shape developed by Pinckney.[12] Streamwise pressure profiles were obtained at a series of radial positions for each pressure ratio. Individual profiles were subsequently digitized and smoothed using a cubic-spline curve-fitting routine and converted into pressure contour maps. The configuration 8 porous centerbody was instrumented with static-pressure ports to determine the surface-pressure distribution.

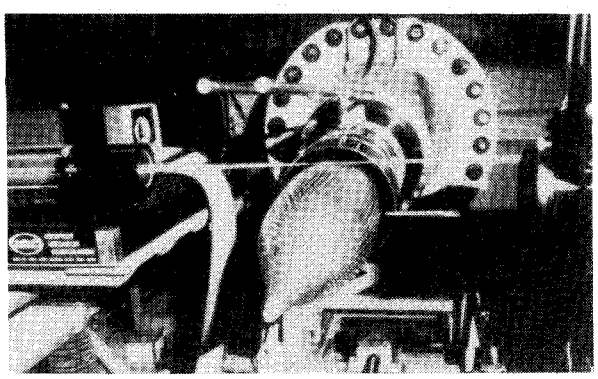

Fig. 2 Apparatus for conducting LDV measurements in a porous-centerbody nozzle flowfield.

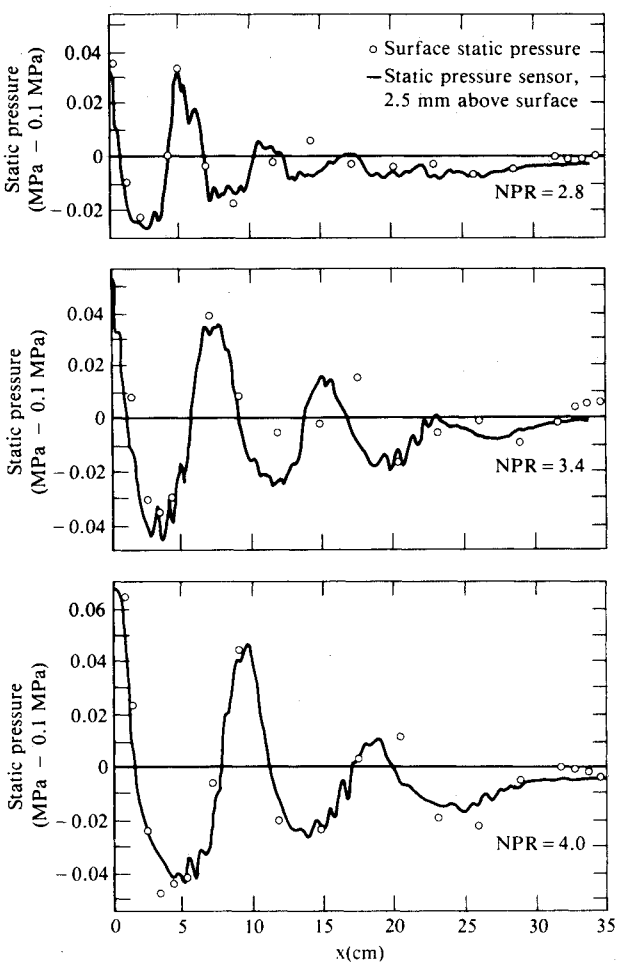

Fig. 3 Comparison between surface static pressure and that sensed by static probe 2.5 mm above centerbody surface for configuration 8.

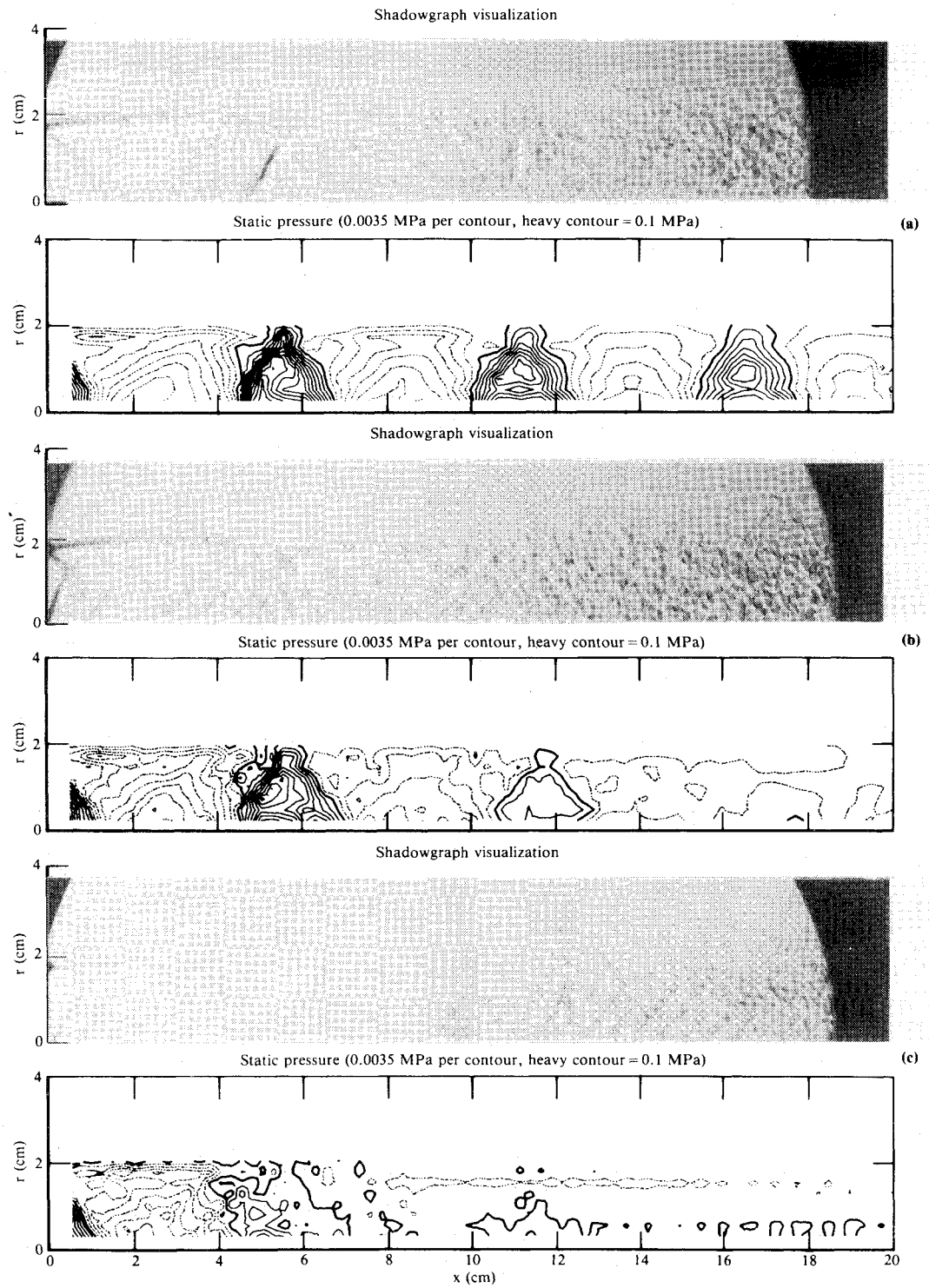

Fig. 4 Shadowgraph photos and static-pressure maps for a) configuration 9T at NPR = 2.8 and $\sigma = 0$; b) configuration 8, NPR = 2.8, $\sigma = 0.027$; and c) configuration 10, NPR = 2.8, $\sigma = 0.057$.

Microphone Measurements

Two near-field microphones were included in the instrumentation to allow comparisons with the acoustic test results. One microphone was located in the nozzle-exit plane 30 cm from the nozzle lip and the second at the same radial distance 30 cm downstream from the exit plane.

Flow Visualization

Instantaneous shadowgraphs were taken for pressure ratios above 1.6 using a spark light source and a 35-mm camera. High-speed shadowgraph movies were taken for each configuration at a pressure ratio of 2.8 using a camera speed of 5000 frames/s.

Results

The spatial resolution of the static-pressure probe was determined to be approximately 2 mm by traversing the probe through the reference nozzle shock system and compensating for the shock jitter observed in the shadowgraph movies. The accuracy of the static-pressure readings was checked by comparing the pressure indicated by the static probe traversed 2.5 mm above the surface of the configuration 8 porous centerbody with the surface static pressure measured at a streamwise row of surface pressure ports. Figure 3 shows good agreement between the two pressure measurements. The small-scale fluctuations in the pressure traces in Fig. 3 are fully reproducible and indicate the fine structure of the pressure field. Small-

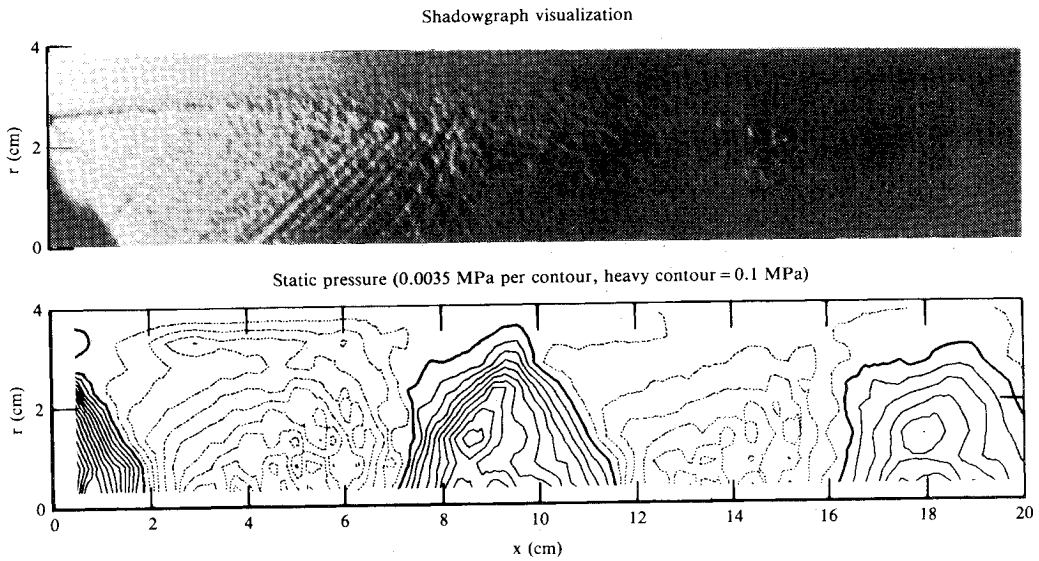

Fig. 5 Shadowgraph photo and static-pressure map for configuration 6 at NPR = 2.8 and $\sigma = 0.027$.

scale pressure fluctuations were present only in the flowfields of the porous centerbodies and were not found in those of the solid centerbody.

Flowfield characterization for each centerbody configuration at a nozzle pressure ratio of 2.8 is given in Figs. 4-6. Two-dimensional static-pressure distributions and streamwise and radial velocities were taken at the midpoint between the centerbody surface and the nozzle lip. Pressure contours were derived from digitized streamwise pressure profiles taken at eight radial locations. The solid and dotted lines represent pressures above and below atmospheric pressure, respectively.

In Fig. 4a, the shadowgraph and the pressure contours show that the flowfield for a solid-surface centerbody (configuration 9T) contains stationary shock cells, positioned at regular intervals along the centerbody and extending from the centerbody surface to the outer edge of the shear layer. This shock cell pattern constitutes the annular equivalent of the diamond-shaped pattern observed in the reference axisymmetric jet. Shadowgraph movies show that the position of the first shock cell oscillates little in the streamwise direction and that the unsteadiness of subsequent cells increase with streamwise distance. The solid centerbody nozzle generates the highest noise levels in the acoustic far field as well as in the near field.

Figures 4b and 4c show flowfield characteristics as modified by the presence of 3% and 6% surface porosity, respectively, consisting of a rectangular pattern of 0.168-cm-diam holes. The data for 3% porosity, Fig. 4b, show that the intensity of the pressure cells decreases rapidly with x, compared with the solid surface centerbody; the pressure cell structure virtually disappears for the 6% porosity centerbody (Fig. 4c). Static pressure varies little from atmospheric pressure throughout the flowfield of the 6% porosity centerbody, although the velocity remains supersonic.

The shadowgraph of Fig. 5 illustrates qualitatively the mechanism whereby porosity attenuates the intense periodic shock cell structure that characterizes the solid centerbody flowfield. These data pertain to the configuration 6 centerbody which has a diameter ratio of 0.53 and porosity of 3%. The first cell is distinct, but its pressure gradients are weaker than those of the first pressure cell of the solid-surface centerbody flowfield (Fig. 4a) because compression is achieved through a series of weak waves associated with the surface holes rather than through a single sharp compression wave. The shock cell structure with 3% porosity is even more diffuse for the larger configuration 8 centerbody (Fig. 4b), and the flowfield of the 6% porosity configuration 10 centerbody consists entirely of a series of weak pressure waves inclined to the

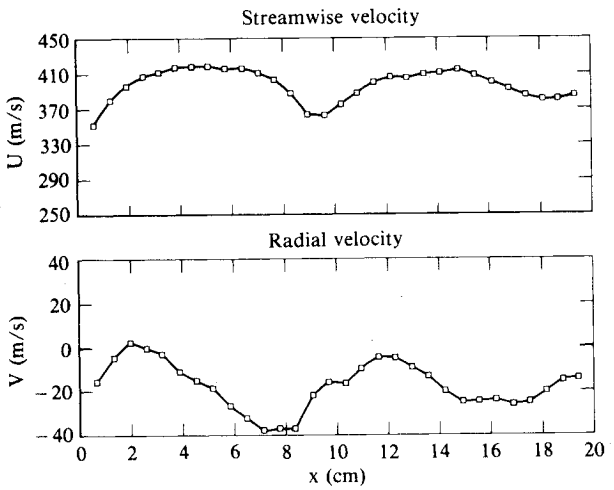

Fig. 6 Streamwise and radial velocities for configuration 6; NPR = 2.8 and $\sigma = 0.027$.

flow at approximately the Mach angle (Fig. 4c). Weak reflections of the pressure waves from the shear layer are also visible in the shadowgraphs. The spacing of the waves in the streamwise direction is precisely that of the surface holes, indicating that the waves are generated by the individual holes. High-speed movies show a steady wave pattern for the entire length of the field of view, especially near the centerbody surface, unlike the solid centerbody pressure cells, where jitter increases with streamwise distance.

Figure 6 shows streamwise and radial velocity data for configuration 6. The velocity profiles based on the LDV and pressure data vary periodically in the streamwise direction, and the velocity values calculated from the pressure data using isentropic relations are virtually identical to those measured. The LDV data for other configurations show similar correspondence with the measured pressure fields.

The resolution of the static-pressure probe was sufficient to discern the pressure variations across the weak waves, which are seen as the small-scale fluctuations in the pressure traces in Fig. 3. Shadowgraphs are sensitive to the second derivative of the density field; thus they emphasize particularly well the small-scale structure of the pressure field. Since the spatial wavelengths of the small- and large-scale pressure field variations differed by approximately an order of magnitude, a digital technique was devised for separating the two com-

ponents using a low-pass digital filter. Details of the filtering procedure are available in Ref. 13. Briefly, a digital Gaussian filter is used to low-pass the pressure data using a wave number cutoff set in accordance with the expected spectral contributions from the surface holes and pressure-cell spacing along the centerbody.

The original and the low-pass-filtered pressure traces are shown in Fig. 7. The large-scale variations were subtracted from the original pressure trace to produce the effectively high-pass-filtered profile shown at the bottom of Fig. 8.

Contour maps (Fig. 8) show the pressure field as well as the filtered large- and small-scale pressure variation. The contours

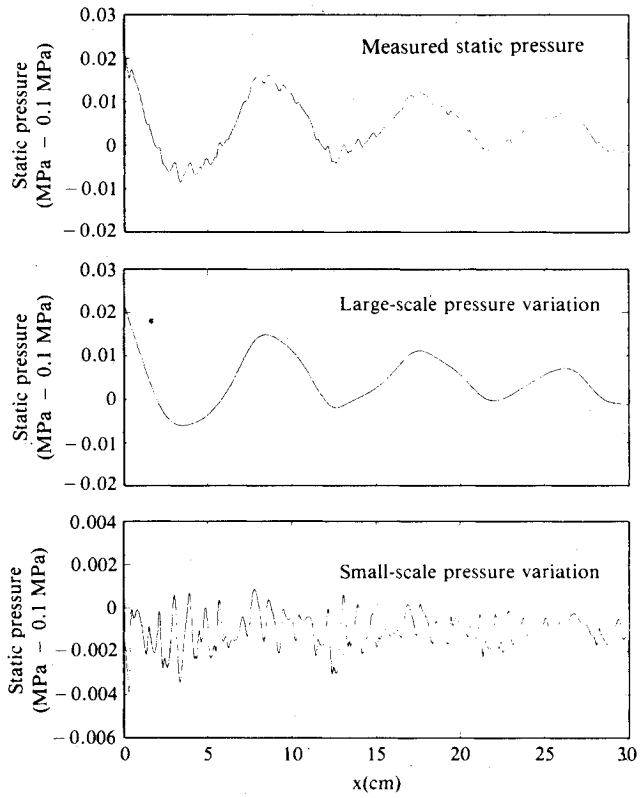

Fig. 7 Decomposition of static-pressure field into large- and small-scale components.

of the small-scale data indicate the existence of a compression wave at 8 cm from the nozzle exit and weak shocks 2-6 cm and 12-16 cm from the nozzle exit. Because of the limited number of pressure traces taken, the contour plotting program is not capable of joining the apparent individual peaks into distinct lines. Comparisons with the corresponding shadowgraphs show the peaks to be part of continuous weak shocks. It is apparent that the waves are strongest in the regions where the large-scale pressure is lowest. The interior of the centerbody communicates with the surrounding air only through the surface holes, and the interior pressure is the average of the surface pressures. The regions of lowest large-scale pressure and highest small-scale pressure variation therefore correspond to regions of outflow from the interior of the centerbody, leading to the conclusion that discrete jets trigger the small-scale pressure wave system.

The large-scale pressure distributions for the three large-diameter-ratio centerbody nozzles are compared in the surface plots in Fig. 9. The corresponding acoustic data indicate that noise suppression effected by the large-diameter-ratio centerbody nozzles is inversely related to the strength and persistence of the large-scale pressure cells. The near-field acoustic measurements showed a consistent 5- to 6-dB variation in the sound level among the configurations, nearly independently of the pressure ratio. The variation is therefore linked to the physical characteristics of the centerbodies, primarily the surface porosity and centerbody-to-nozzle diameter ratio. Surface porosity did not appear to be important for subsonic flows.

Figure 10 shows the Mach number dependence of the length of the first cell L_1, normalized with the nozzle-exit height h. The data for the various centerbody geometries exhibit similar linear Mach number dependence. The length of the pressure cells also varies with the distance along the centerbody. In Fig. 11 the normalized cell length is plotted as a function of cell number. Although the solid centerbody produces more identifiable cells than centerbodies with surface pores, the decrease in cell length with cell number is similar for all nozzle configurations. The decrease in cell spacing can be attributed to the approximately linear growth of the shear layer thickness with streamwise distance, which effectively reduces the cross-sectional area of the high-speed core flow. The observed spatial variation of the pressure cells is consistent with a system of compression/expansion waves that is reflected from the centerbody surface and the shear layer. Ribner[14] proposed that the solid portions of the surface reflect an expansion wave

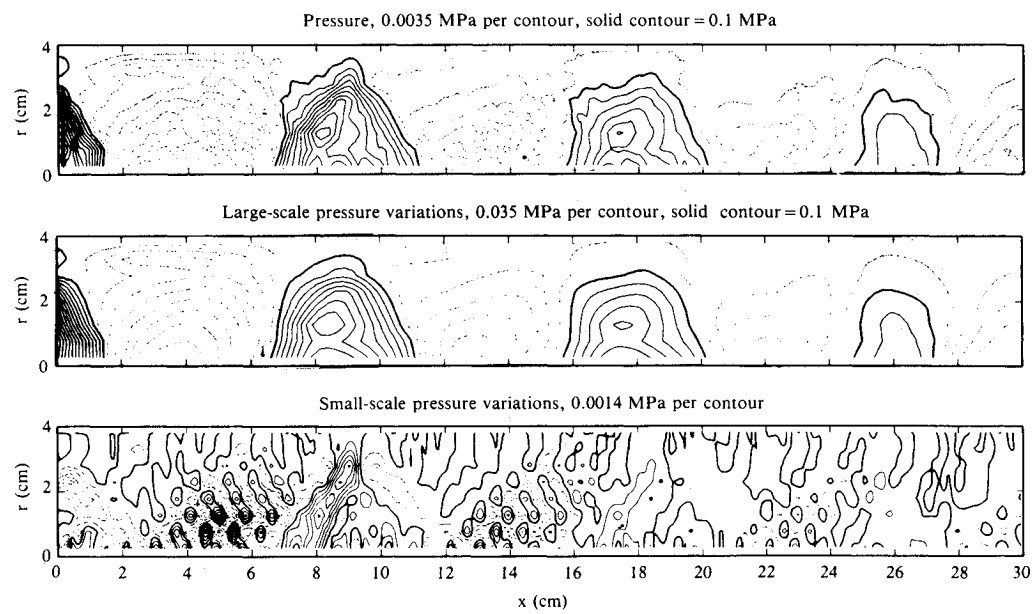

Fig. 8 Comparison of static pressure with large- and small-scale variations for configuration 6 at a nozzle-pressure ratio of 2.8.

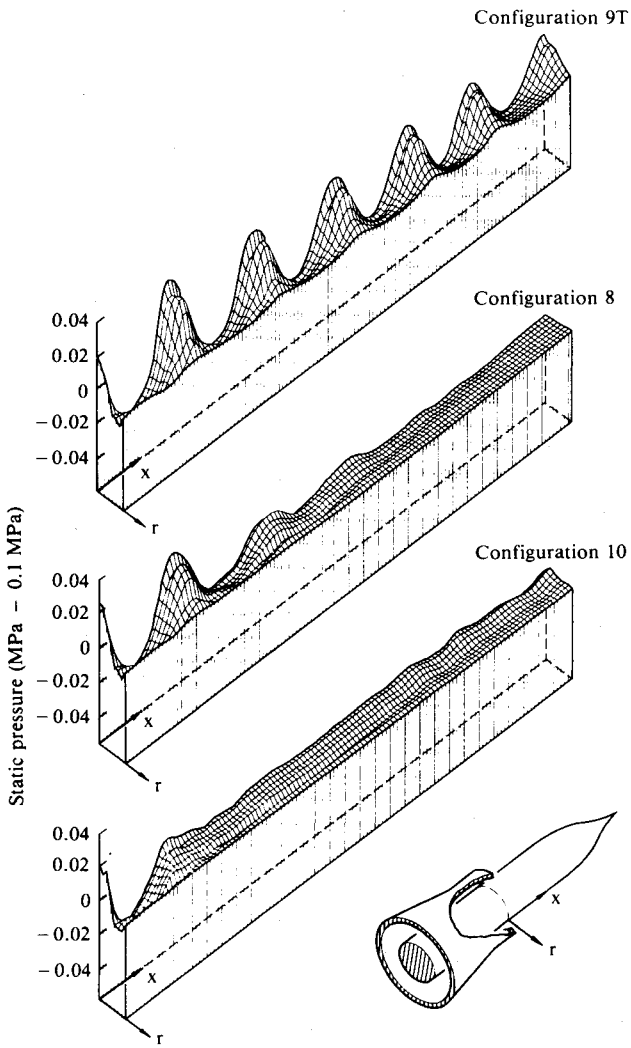

Fig. 9 Comparison of static-pressure distributions at a nozzle-pressure ratio of 2.8.

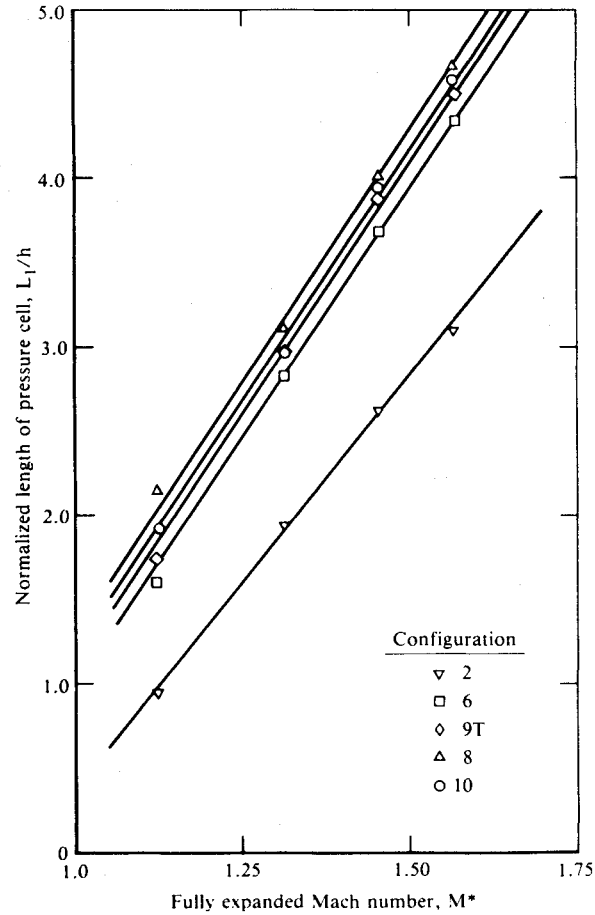

Fig. 10 Variation in length of first pressure cell with increasing Mach number.

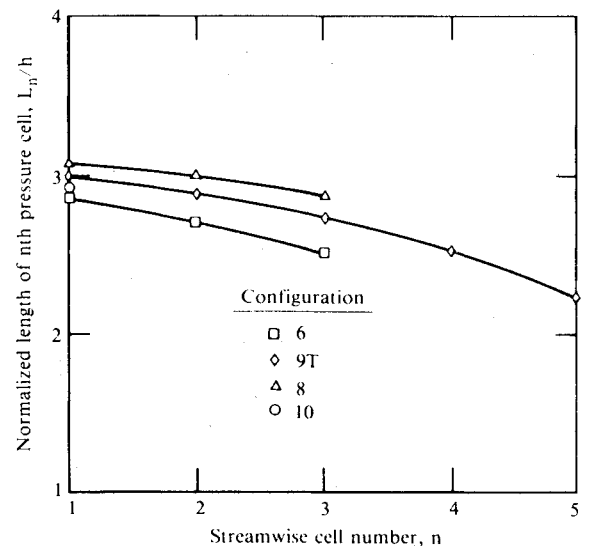

Fig. 11 Streamwise variation of pressure-cell length at a nozzle-pressure ratio of 2.8.

as an expansion and the pores act as soft surfaces, reflecting it as a shock. With appropriate surface porosity, the reflected shock/expansion waves mutually cancel, and the net reflection of an impinging expansion wave is negligible.

Figure 12 shows the normalized pressure ratio across compressions and expansions for successive pressure cells. The ratio $(P_2-P_1)/P_1$ is equivalent to shock strength, where P_1 is the pressure on the low-pressure side of a compression or an expansion and P_2 is the corresponding pressure on the high-pressure side. The rate of decay of cell strength increases with porosity, and for identical porosity the decay is faster for the larger centerbody-to-nozzle diameter ratios.

In Fig. 13 the acoustic far-field data reported by Bauer[10] are presented as a function of the strength of the first compression wave. The data collapse to a single line, indicating a simple, direct relation between the noise level and the strength of the first pressure cell for all centerbody geometries. For example, the overall sound pressure level (OASPL) for the configuration 10 nozzle at nozzle-pressure ratio (NPR) = 4.0 is approximately equal to that of nozzle configuration 9T at NPR = 2.8 because the pressure increase through the first compression is nearly the same for both cases.

Discussion and Conclusions

The intense shock cells, which appear as the annular centerbody-nozzle equivalent of the circular jet shock pattern, are strongly attenuated by the presence of a porous surface. The shock cells are replaced by a system of weak waves that originates at, and is locked to, the surface holes; its intensity is strongest in the regions of outward flow of air from the centerbody interior. The supersonic flowfield of the nozzle that was most effective in reducing noise (configuration 10) consisted of a series of weak waves with no evidence of shock cells. For circular supersonic jets, the nozzle must be operated at the precise design pressure-ratio to achieve parallel streamlines at the nozzle-exit plane and thereby an absence of shocks throughout the flowfield. Parallel streamlines appear to be

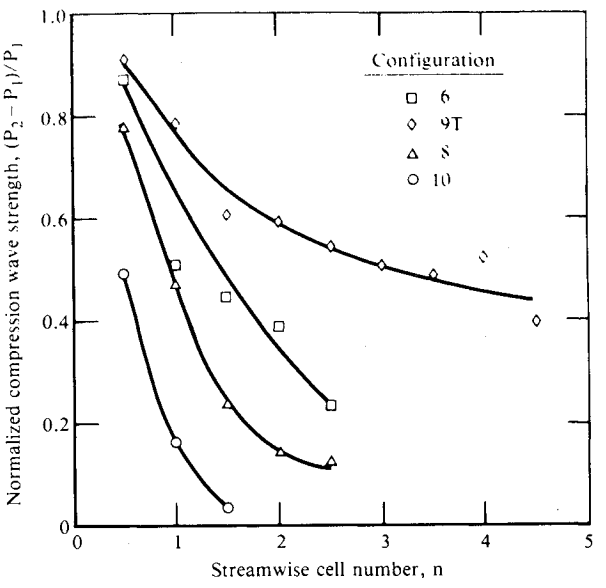

Fig. 12 Streamwise variation of pressure-cell strength at a nozzle-pressure ratio of 2.8.

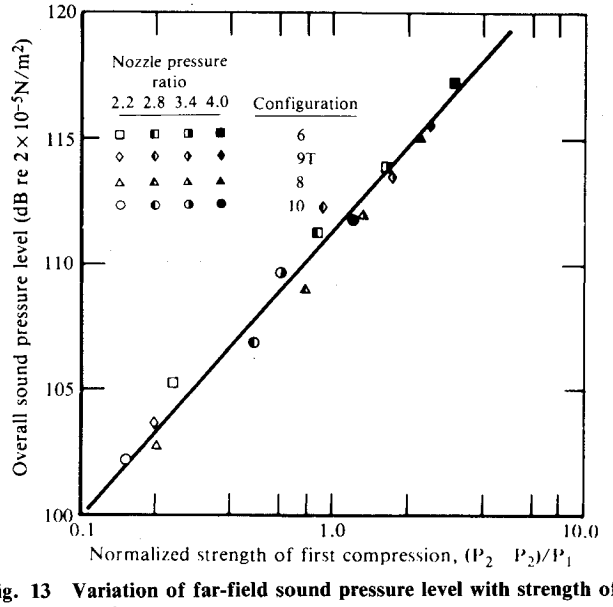

Fig. 13 Variation of far-field sound pressure level with strength of first compression.

achievable with the porous-centerbody nozzle for the full range of supersonic nozzle pressure ratios tested. For the 6% porosity centerbody, the series of weak shocks induced by the surface holes appears to adjust at all pressure ratios to produce alignment of streamlines with the system centerline after the initial expansion wave. The deceleration to subsonic velocities occurs through the viscous action of the surface boundary layer and the external shear layer.

Observation of the porous-centerbody flowfields shows that with increasing porosity, a system of variable-intensity weak waves is established and tends to diffuse the pressure gradients of the shock cells, reducing the associated large-scale surface pressure variations. This effect also reduces the pressure differentials across the wall of the centerbody that produce inward or outward flow through the surface holes and control the intensity of the weak wave system. It appears that, for sufficient wall porosity, a self-correcting adjustment of the weak shocks occurs in response to the initial expansion fan at any pressure ratio, resulting virtually in a perfectly expanded flow at atmospheric pressure along the centerbody.

The overall sound pressure level (OASPL) of the porous-centerbody nozzles scales with the strength of the first compression wave. The quantity represented by the OASPL is a global measurement that sums the contributions of all noise sources in a given direction. The intensity of the first compression wave must therefore be taken as a measure of the effectiveness of the entire subsequent shock system as a noise generator. Seiner and Norum[4] hypothesized that the mechanism for broadband shock-noise generation in a supersonic jet consists of the interaction of the shear-layer turbulence with the pressure gradients of the shock cells, and showed that the most intense sound is generated by the third or fourth shock cell. In the simplest approximation, we can define shock-noise generation efficiency to be a function of the product of shock-cell intensity and the thickness and degree of coherence of the mixing layer. If we further assume the interaction of the shear layer with a shock cell has no substantial effect on the shear layer's growth rate or turbulent eddy distribution, then this hypothesis is consistent with the observed noise-reduction effects of the porous-centerbody nozzle. The linearly growing shear layer is thin as it intersects the first compression wave, and it therefore generates little acoustic energy. If the subsequent shock cells have been eliminated by the presence of the porous centerbody, then the thickened shear layer encounters no further intense pressure gradients, and shock noise is minimized.

More data are needed to determine whether porosity per se leads to flow modification, or whether the size and particular distribution of surface holes play a role in generating weak wave fronts, which interact with the shear layer to attenuate shock cells that otherwise would be present. The next step in continuing this investigation would be to examine merging of individual shock fronts in three dimensions and follow their interaction with the shear layer to obtain guidance for optimizing specific means of introducing porosity.

Acknowledgments

This work was performed under NASA Langley Research Center Contract NAS1-16284.

References

[1]Maestrello, L., "Initial Results of a Porous Plug Nozzle for Supersonic Jet Noise Suppression," NASA TM-78802, 1978.

[2]Maestrello, L., "An Experimental Study on Porous Plug Jet Noise Suppressors," AIAA Paper 79-0673, 1979.

[3]Das, I., Matambo, T. J., and Dosanjh, D. S., "Aeroacoustics of Supersonic Porous Plug-Nozzle Flows," AIAA Paper 83-0775, 1983.

[4]Seiner, J. M. and Norum, T. D., "Aerodynamic Aspects of Shock Containing Jet Plumes," AIAA Paper 80-0965, 1980.

[5]Pao, P. S. and Seiner, J. H., "A Theoretical and Experimental Investigation of Shock-Associated Noise in Supersonic Jets," AIAA Paper 81-1973, 1981.

[6]Seiner, J. M. and Yu, J. C., "Acoustic Near Field and Local Flow Properties Associated with Broadband Shock Noise," AIAA Paper 81-1975, 1981.

[7]Lighthill, M. J., "On the Energy Scattered from the Interaction of Turbulence with Sound or Shock Waves," *Proceedings of the Cambridge Philosophical Society*, Vol. 49, 1953, pp. 531-551.

[8]Howe, M. S. and Ffowcs Williams, J. E., "On the Noise Generated by an Imperfectly Expanded Supersonic Jet," *Philosophical Transactions of the Royal Society of London*, Vol. A289, 1978, pp. 271-314.

[9]Tanna, H. K., Tam, C. K. W., and Brown, W. H., "Shock Associated Noise Reduction from Inverted-Velocity-Profile Coannular Jets," NASA CR-3454, 1981.

[10]Bauer, A. B., "Jet Noise Suppression by Porous Plug Nozzles," AIAA Paper 81-1993, 1981.

[11]Bauer, A. B., Kibens, V., and Wlezien, R. W., "Jet Noise Suppression by Porous Plug Nozzles," NASA CR-3613, 1982.

[12]Pinckney, S. Z., "A Short Static-Pressure Probe Design for Supersonic Flow," NASA TN D-7978, 1975.

[13]Kibens, V. and Wlezien, R. W., "Porous-Plug Flowfield Mechanisms for Reducing Supersonic Jet Noise," AIAA Paper 83-0774, 1983.

[14]Ribner, H. S., "Perspectives on Jet Noise," *AIAA Journal*, Vol. 19, Dec. 1981, pp. 1513-1526.